RSC Advances

PAPER

View Article Online
View Journal | View Issue

Cite this: *RSC Adv.*, 2016, **6**, 53430

Magnetically separable $CuFe_2O_4$/reduced graphene oxide nanocomposites: as a highly active catalyst for solvent free oxidative coupling of amines to imines†

Ritu Dhanda and Mazaahir Kidwai*

In this report, a very simple and straightforward one step coprecipitation method was used for decorating $CuFe_2O_4$ nanoparticles (NPs) over graphene sheets. The as synthesized $CuFe_2O_4$/RGO nanocomposites (CFRNCs) were fully characterized by XRD, TEM, HRTEM, XPS, FTIR, Raman, ICP-AES and SEM-EDS analysis which shows well controlled small sized (~7 nm from Scherrer formula) $CuFe_2O_4$ NPs with dense and compact loading over RGO sheets. The magnetic study reveals the superparamagnetic behavior of ferrite NPs which provides an extra benefit in catalytic recyclability. The synthesized CFRNCs were found to be highly active in aerobic oxidative coupling of amines to desired imines achieving excellent yields (88–95%) under mild reaction conditions. Moreover the role of Cu, Fe species and their interaction with RGO sheets was well studied separately by synthesizing CuO/RGO, Fe_2O_3/RGO, bare $CuFe_2O_4$ and RGO samples, then catalytic mechanism was proposed based upon various controlled reaction results. The CFRNCs were recycled up to 4th cycle under similar catalytic conditions and found to be highly efficient without any accountable loss in activity and stability. This outstanding activity of CFRNCs can be attributed to synergistic coupling between Cu/Fe species, high surface area due to the presence of RGO sheets and small sized surfactant free $CuFe_2O_4$ NPs which led to the use of the present nanocatalyst in many more industrially important catalytic applications.

Received 6th April 2016
Accepted 19th May 2016

DOI: 10.1039/c6ra08868f

www.rsc.org/advances

1 Introduction

The environmental problems concerning organic waste have increased due to industrial development and waste accumulation which pollutes the environment and is harmful to human health. Due to these concerns, solvent free organic synthesis are of great importance in industrial processes with minimum organic waste.[1,2] Among various solvent free couplings, amine to imine conversion is one of the important processes due to application of its products in the synthesis of diverse intermediates for a variety of fine chemicals, pharmaceuticals and molecular motors.[3,4] Among the various reported methods, oxidative coupling of amines to imines provides an attractive alternative for imine synthesis. Recently, various heterogeneous materials have been designed for catalyzing this coupling reaction.[5–10] However, various key challenges like harsh reaction conditions, low selectivity and involvement of organic solvents still exist. Since the separation and purification of unstable imines and catalyst is very difficult and brings environmental issues hence it is very desirable to develop highly selective and cost-effective heterogeneous catalysts which can work under solvent-free conditions and easily separated after reaction.

Keeping environmental issues in mind, various magnetic nanomaterials were designed for organic synthesis reactions which are easy to recover and reusable for various cyclic runs. Among magnetic NPs, ferrites with general formula MFe_2O_4 (M is divalent transition metal, such as Mn, Fe, Co, Ni, Cu, Zn *etc.*) are one of the best nanomaterials for catalytic reactions because their properties can be varied by changing the identity of the divalent M^{2+} ion. Among the ferrites, $CuFe_2O_4$ has received great attention due to large abundance, low cost, environmental friendly nature and highly active Cu(II) cation for catalysis reaction. In recent years, $CuFe_2O_4$ NPs were used in various catalysis reactions like steam reforming, nitroaromatic reduction, dye degradation, acyloxylation, phenol hydroxylation *etc.*[11–20] In general, it has been found that loading of these ferrites NPs on reduced graphene oxide (RGO) sheets leads to highly active and selective catalysts.[21–24]

Green Chemistry Research Laboratory, Department of Chemistry, University of Delhi, North campus, New Delhi-110007, India. E-mail: kidwai.chemistry@gmail.com; Fax: +91-11-27666235

† Electronic supplementary information (ESI) available: XRD spectra for CuO/RGO, bare $CuFe_2O_4$ and GO samples. SEM-EDS analysis for $CuFe_2O_4$/RGO nanocomposites. Survey spectrum of XPS and high resolution C 1s spectrum. The TGA analysis of CuO/RGO NCs. The low resolution TEM analysis for $CuFe_2O_4$/RGO NCs with varying graphene content and bare $CuFe_2O_4$ NPs. ^1H and ^{13}C NMR of synthesized imine compounds and table showing comparison of present catalyst with earlier reports. See DOI: 10.1039/c6ra08868f

Since, graphene is two-dimensional sp^2 carbon network which has remarkable electronic conductivity (10^5 to 10^6 S m^{-1}), large surface area (2000–3000 m^2 g^{-1}), excellent absorptivity, ultrathin thickness, superior structural flexibility, low manufacturing cost, exceptional mechanical, optical, thermal and magnetic properties which makes it a most promising support material for use in diverse horizons like sensors, electronics, electrochemical energy storage, efficient catalysis *etc.*[25–31] Graphene sheets can be prepared in large scale by oxidative exfoliation of common graphite to graphene oxide (GO) *via* Hummer's method and followed by chemical or thermal reduction. Various metals and metal oxides NPs were anchored on graphene sheets *via* co-reduction, co-precipitation method which showed enhanced properties and improved functionalities due to interaction between NPs and graphene sheets.[21–24,32]

Recently, $CuFe_2O_4$/RGO nanocomposites were synthesized under hydrothermal condition using high temperature and long reaction time.[21–24] However, in this report we have synthesized reduced graphene oxide supported $CuFe_2O_4$ NPs *via* facile and inexpensive co-precipitation approach at low reaction temperature. The synthesized CFRNCs were well characterized by XRD, TEM, HRTEM, SEM-EDAX, VSM, XPS, ICP-AES, FTIR and Raman spectroscopy. The $CuFe_2O_4$ NPs were found to be in pure phase, small sized and homogeneously distributed all over graphene sheets. The NCs exhibits excellent magnetic properties that help in easier separation of present nanocatalyst. The CFRNCs were applied in solvent free oxidative coupling of amines to imines and found to be highly active and selective for desired product. Moreover, this catalyst was found applicable for oxidative coupling of both electron donating and electron withdrawing groups containing amines. The NCs can be magnetically recycled and showed very good recyclability for amine to imine conversion for continuous cyclic runs which may lead to the use of present nanocatalyst in many more industrially important catalytic applications.

2 Experimental

2.1. Chemicals and materials

Copper(II) nitrate trihydrate (99%), iron(III) nitrate nonahydrate (98%), 4-chlorobenzylamine (98%) and natural flake graphite were purchased from Sigma Aldrich USA. 2-Methylbenzylamine (98%), 4-(trifluoromethyl)benzylamine (98%), 4-fluorobenzylamine (97%), 3-(trifluoromethyl)benzylamine (97%), 2-chlorobenzylamine (96%), 2-methoxybenzylamine (98%), 3-methoxybenzylamine (98%), 4-methylbenzylamine (98%), 4-methoxybenzylamine (98%), 3,4-dichlorobenzylamine (96%) and benzylamine (99%) were from Alfa Aesar. Sodium hydroxide pellets (97.5%) was from Thomas baker. All chemicals were used as received without any further purification. Deionized water was used in all experiments. GO was synthesized from natural graphite powder following improved Hummers method.[33]

2.2. Synthesis of $CuFe_2O_4$ nanoparticles on RGO nanosheets

The $CuFe_2O_4$/RGO NCs with different RGO (15, 30, 45, 60 wt%) content has been synthesized by one pot coprecipitation method. The typical experimental procedure for synthesis of CFRNCs with 30 wt% graphene is as follows: 100 mg of GO was dispersed in 80 mL of water *via* ultra-sonication. Subsequently, 1 mmol of $Cu(NO_3)_2 \cdot 3H_2O$ and 2 mmol $Fe(NO_3)_3 \cdot 9H_2O$ (molar ratio of Cu : Fe = 1 : 2) was dissolved in 20 mL of water and then dropwise added to the GO dispersion. The resulting reaction mixture was magnetically stirred for 10 minutes. Then freshly prepared aqueous NaOH (8 M) was added drop wise to the reaction mixture to maintain pH 10. The whole setup was maintained at room temperature and stirred for 15 minutes. Then resulted mixture was refluxed at 80 °C for next 2.5 h. The resulted dark brown product was isolated by centrifugation, washed with water for three times and then dried in oven at 50 °C. For comparison, bare $CuFe_2O_4$ NPs were also synthesized using similar procedure without addition of GO.

2.3. Synthesis of CuO/RGO NCs

For synthesis of CuO/RGO with similar percentage loading (~30 wt% graphene), 3 mmol of $Cu(NO_3)_2 \cdot 3H_2O$ was taken and followed by similar reaction procedure as used in synthesis of CFRNCs.

2.4. Synthesis of hematite-reduced graphene oxide nanocomposites (NCs)

The reduced graphene oxide (RGO) supported alpha-Fe_2O_3 nanoparticles (30 wt% graphene) were synthesized *via* the earlier reported method.[34]

2.5. Synthesis of RGO nanosheets

For synthesis of reduced graphene oxide sheets, 100 mg of GO was dispersed in 100 mL of water *via* ultra-sonication. Then resulted mixture was refluxed at 80 °C for next 2.5 h. The resulted dark brown product was isolated by centrifugation, washed with water for three times and then dried in oven at 50 °C.

2.6. Catalytic oxidative coupling of benzylamine to imine

The oxidation of benzylamine was performed using O_2 as oxidant under solvent free conditions. Typically 15 mg of catalyst and 1 mmol of benzylamine were taken in a 10 mL round bottom flask. The reaction mixture was then heated at 60 °C for the required time under O_2 balloon and the progress of reaction was monitored by thin layer chromatography (TLC). After reaction, catalyst was magnetically separated and the filtrate was passed through the basic alumina-packed column using a mixture of ethyl acetate and hexane (1 : 9) as eluent. The imine derivatives obtained by this procedure were characterized by ^1H and ^{13}C NMR.

2.7. Characterization

The phase purity and crystal structure of synthesized samples were examined using powder X-ray diffraction (XRD, Bruker D8 Advance diffractometer) with Cu Kα as a radiation source (λ = 1.5406 Å) at a scanning rate of 3° min^{-1}. The TEM and HRTEM images were obtained from Phillips Technai G^2 30 transmission electron microscope operating at 200 kV accelerating voltage.

TEM samples were prepared by putting a drop of sample dispersion in ethanol on carbon coated copper grid and allowing the solvent to evaporate at room temperature. Elemental composition was determined by SEM-EDS and ICP-AES. EDS was recorded on energy dispersive spectrometer attached with JEOL JSM-6610LV scanning electron microscope (SEM). ICP-AES was done using ARCOS system from M/s. Spectro, Germany. The X-ray photoelectron spectroscopy measurement was performed using SPECS XPS system. Magnetic properties of $CuFe_2O_4$/RGO nanocomposite sample were measured by vibrating sample magnetometer (Micro-Sense EV9) at room temperature (20 ± 1 °C). Raman study was done using Renishaw inVia Raman spectrometer equipped with a laser having a wavelength of 514 nm. Fourier transform infrared (FTIR) spectra (KBr disk, 4000–400 cm^{-1}) were recorded on a Perkin Elmer FT-IR 2000 spectrophotometer.

3 Result and discussion

The phase purity and crystal structure of $CuFe_2O_4$ NPs and successive reduction of GO to RGO was examined by powder XRD studies. Fig. 1a display the XRD spectrum of CFRNCs where all the peaks can be assigned to cubic $CuFe_2O_4$ spinel structure without any impurity peaks of copper oxides (Cu_2O or CuO).[21–24] From XRD studies, it was found that GO exhibits two peaks at $2\theta = 10.03$ and 42.5° corresponding to (001) and (002) planes (see Fig. S1a†) while after reduction GO exhibits a broad peak at 20° corresponding to (002) planes of graphene sheet.[21,22,33] However, no RGO peaks was found in XRD spectrum of CFRNCs indicating that GO was exfoliated due to crystal growth of $CuFe_2O_4$ NPs between interlayer of graphene oxide sheets.[21–23] The diffraction peaks at $2\theta = 30.2$, 35.5, 37.5, 43.2, 47.7, 57.3, 62.4 & 71.2° can be indexed to 220, 311, 222, 400, 331, 511, 440 and 620 planes of cubic $CuFe_2O_4$ spinel structure (JCPDS 25-0283). The broad diffraction peaks of CFRNCs indicates smaller size of NPs which was found 7 nm from Scherrer formula. For controlled catalytic studies, bare $CuFe_2O_4$ and CuO/RGO were synthesized separately under similar reaction conditions and characterized by powder XRD analysis (see Fig. S1b and c† for XRD spectra). The bare copper ferrite NPs exhibits diffraction peaks at 29.9, 35.4, 36.9, 57.8 and 62.2° which corresponds to cubic $CuFe_2O_4$ spinel structure while peaks 38.7 and 48.5°can be indexed as impurity peak corresponding to heterogeneous growth of CuO particles (JCPDS 80-1268). These findings indicates that GO sheets not only stabilize the NPs but also helps in controlled synthesis of pure $CuFe_2O_4$ NPs. The CuO/RGO sample exhibit diffraction peaks at 32.4, 35.4, 38.4, 48.3, 53.4, 69.1, 61.5, 66.1, 67.7, 72.3 and 74.7° can be assigned to monoclinic CuO (JCPDS card no. 48-1548) without any impurity peaks.

The effective reduction of GO to RGO and successful synthesis of RGO supported $CuFe_2O_4$ NPs can be further

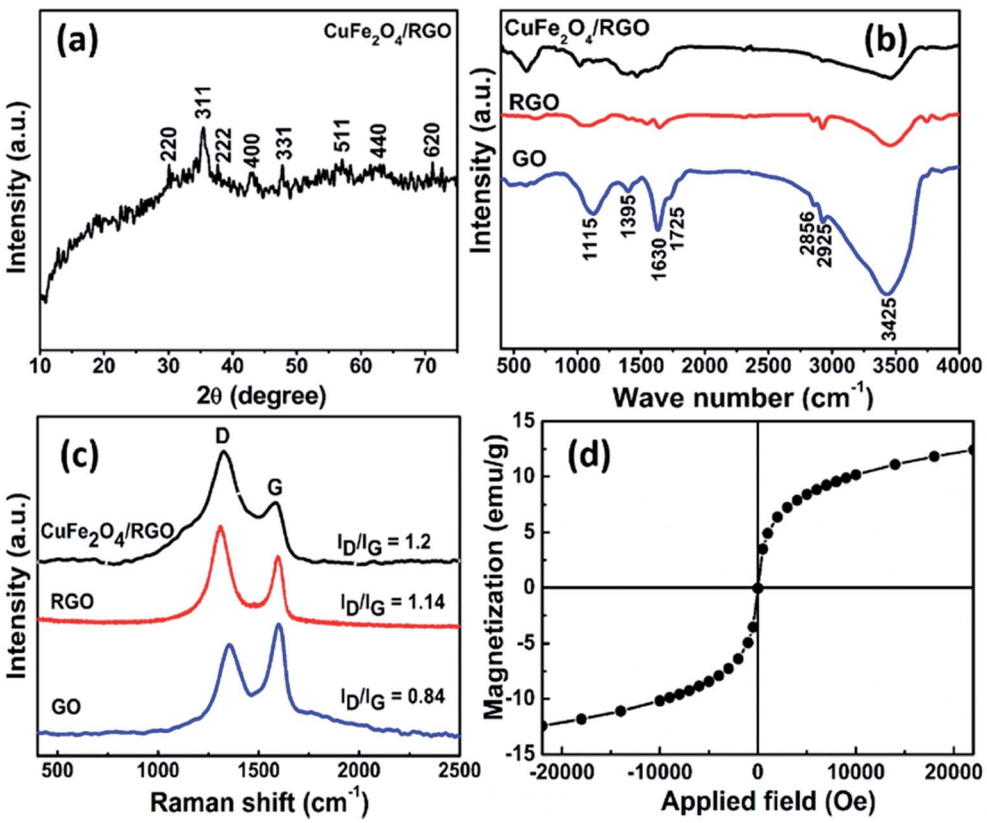

Fig. 1 (a) Powder XRD spectrum of CFRNCs in the range of 10 to 75°, (b) FTIR and (c) RAMAN spectra of GO, RGO and CFRNCs samples. (d) Hysteresis loop for CFRNCs.

explained by the FTIR and Raman studies. Fig. 1b represents the FTIR spectra of GO, RGO and CFRNCs samples. The FTIR spectrum of GO clearly shows the abundance of oxygen containing groups. For GO, the broad absorption at 3425 cm^{-1} can be assigned to O–H stretching vibration. The other peaks at 1725, 1395 and 1125 cm^{-1} appears due to C=O stretching mode, O–H bending mode and C–O (alkoxy) stretching mode. The peaks centered at 2856 and 2925 cm^{-1} in the GO spectrum also remain prominent in RGO and CFRNCs can be assigned to $-CH_2$ stretching vibrations of graphene sheets. The peak at 1630 cm^{-1} in GO is due to the stretching vibration of absorbed water molecule on graphene oxide sheets while the absence of this peak in CFRNCs indicates complete removal of adsorbed water molecules.[35] The FTIR spectrum of both RGO and CFRNCs sample show a decrease in absorption intensity for O–H group (3425 cm^{-1}) and absence of absorption peak corresponding to C=O (1725 cm^{-1}), C–O (1125 cm^{-1}) stretching vibrations and O–H bending (1395 cm^{-1}) vibrations. These results clearly indicate that GO has been reduced up to a great extent. A new absorption peak at 602 cm^{-1} in case of CFRNCs can be assigned to metal oxygen bonds.

Raman spectroscopy is a powerful technique in characterization of structural properties of carbon based materials. Fig. 1c represents the Raman spectra of GO, RGO and CFRNCs. As shown in Raman spectrum, GO display two prominent peaks at 1354 cm^{-1} and 1600 cm^{-1} corresponding to D and G band of carbon respectively. The small shifting was observed in D and G bands of RGO and CFRNCs indicating increase in disorderness and removal of oxygen containing functional groups from graphene oxide sheets. It is well known that D band can be assigned to disordered structure or defects in graphene sheets while G band is associated with E_{2g} mode observed for sp^2 carbon domains.[36] The calculated intensity ratio of D and G band (I_D/I_G) for CFRNCs ($I_D/I_G = 1.2$) shows higher value over RGO ($I_D/I_G = 1.14$) and GO ($I_D/I_G = 0.81$) which suggests that conjugated graphene network (sp^2) is re-established after loading of $CuFe_2O_4$ NPs on GO sheets resulting increased I_D/I_G value for nanocomposites.[33]

Magnetic properties of as synthesized CFRNCs were investigated at room temperature (20 ± 1 °C) using a vibrating sample magnetometer with an applied magnetic field of −22 000 Oe to 22 000 Oe and corresponding hysteresis loop is shown in Fig. 1d which clearly reveals superparamagnetic nature for nanocomposites representing behavior of ferrite structure.

The size, morphology and crystal structure of CFRNCs were further studied by TEM and HRTEM. From low resolution TEM, it was observed that $CuFe_2O_4$ NPs are distributed all over RGO sheets, however some agglomerations were also found which may be due to magnetic interaction between surfactant free $CuFe_2O_4$ NPs and high percentage loading (Fig. 2a and b). The NPs were not observed outside the RGO sheets indicating very good interactions between NPs and RGO sheets. The average particle size for $CuFe_2O_4$ NPs supported on RGO sheets was found ~12 ± 2 nm with addition of very small $CuFe_2O_4$ crystallites. For further study, HRTEM analysis was done on

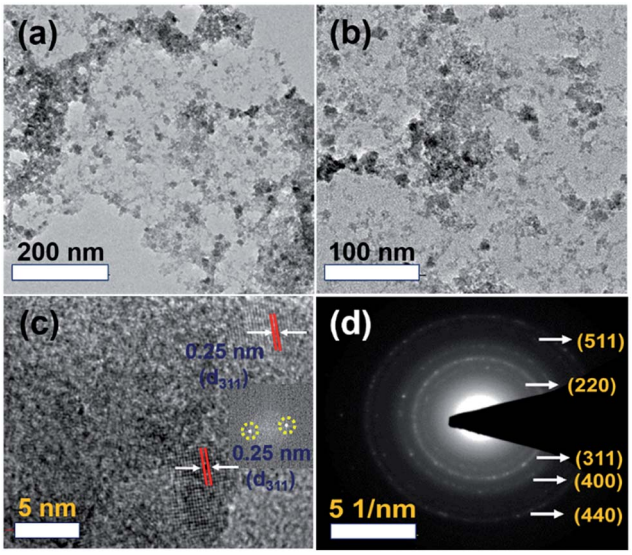

Fig. 2 (a and b) Low resolution TEM images, (c) high resolution TEM showing interplanar distance (inset: 2D-FFT showing exposure of (311) plane) and (d) SAED pattern for as prepared CFRNCS.

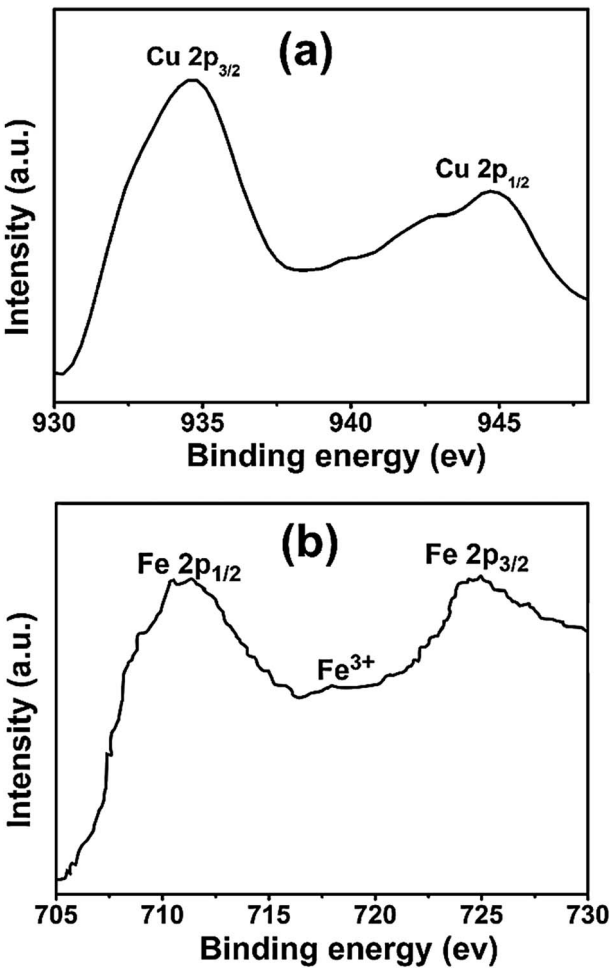

Fig. 3 High resolution XPS spectrum of (a) Cu 2p and (b) Fe 2p levels in CFRNCs.

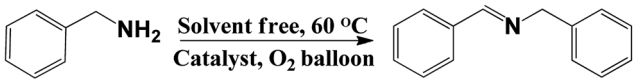

Scheme 1 Oxidative coupling of benzylamine to *N*-benzylidene-1-phenylmethanamine.

CFRNCs which reveals crystalline structure of as synthesized RGO supported $CuFe_2O_4$ NPs. The interplanar spacing (d_{hkl}) was calculated from adjacent lattice fringes was found to be 0.25 nm which can be indexed to (311) plane of cubic spinel $CuFe_2O_4$ (Fig. 2c).[21,22] The two dimensional Fast-Fourier transform (2D-FFT) pattern calculated for $CuFe_2O_4$/RGO sample is shown in Fig. 2c inset also confirmed the exposure of (311) plane for $CuFe_2O_4$ nanoparticles. The SAED pattern of CFRNCs is shown in Fig. 2d which represents the crystalline nature of the particles with the cubic structure, where the (220), (311), (400), (511) and (440) lattice planes were clearly indexed in agreement with XRD results. The elemental analysis was carried out on $CuFe_2O_4$/RGO nanocomposites using SEM EDS and obtained results are shown in Fig. S2.† The EDS results confirmed the presence of Cu, Fe, C and oxygen as main elements. The Cu/Fe ratio obtained from EDS was found to be consistent with stoichiometric elemental ratios for $CuFe_2O_4$. The carbon element detected in EDS would come from RGO sheets while oxygen was detected from $CuFe_2O_4$ NPs and residual oxygen containing functional groups on RGO sheets. The actual elemental composition and percentage loading for CFRNCs were further analyzed by ICP-AES study. ICP analysis of 10 mg sample showed 1.96, 3.47 mg of Cu and Fe elements (*i.e.* 19.6% and 34.7%) respectively which means 7.4 mg of $CuFe_2O_4$ was loaded on graphene sheets (*i.e.* 26% graphene content). ICP findings further confirmed that Cu and Fe are present in 1 : 2 molar ratio which is consistent with stoichiometry of $CuFe_2O_4$ structure. The percentage loading of CuO/RGO was studied by thermogravimetric technique which display 23 wt% graphene content in NCs (see Fig. S3†).

The elemental composition and surface oxidation state of CFRNCs were further examined by XPS. Fig. S4a† display the survey spectrum of CFRNCs which reveals the presence of C, O, Cu and Fe as the main element. For further investigation, high resolution XPS was done for C 1s, Cu 2p and Fe 2p core levels and spectrum is shown in Fig. S4b† and 3(a and b) respectively. High resolution deconvoluted C 1s spectrum display four peaks centered at 284.8, 286.5, 288.2, 289.2 eV corresponding to C–C/C=C/C–H, C–OH, C=O and O=C–O bonds of sp^2 carbon of RGO sheets respectively.[33] For C 1s spectrum, high intensity of C–C/C=C/C–H peak was found over C–OH, C=O and O=C–O peaks indicating exclusive reduction of GO to RGO. The Cu 2p core level spectrum show Cu $2p_{3/2}$ and Cu $2p_{1/2}$ peaks centered at 934.7 and 944.6 eV binding energies which is in conformity with the earlier reported results.[21–23] The Fe 2p core level spectrum display two peaks at 711.2 and 724.8 eV which can be assigned as $2p_{3/2}$ and $2p_{1/2}$ peaks. Additionally, Fe 2p spectrum show a weak satellite at 718.3 eV which indicates presence of Fe^{3+} cations as earlier reports of copper ferrite.[21–23] Hence obtained results indicate controlled synthesis of pure spinel $CuFe_2O_4$ NPs supported on reduced graphene oxide sheets.

3.1. Catalytic study

To explore the catalytic activity of as synthesized CFRNCs, solvent free oxidative coupling of benzylamine in presence of O_2 balloon was chosen as a model reaction for developing the optimal reaction conditions (Scheme 1). First the reaction was performed with $CuFe_2O_4$/RGO NCs at 60 °C and progress of the reaction was monitored by thin layer chromatography. The obtained imine product was well characterized by ^1H, ^{13}C NMR and mass spectrometry (see Fig. S7–S9†). The CFRNCs showed excellent activity (>95%) and remarkable selectivity for benzylamine coupling to desired imine product after 8 h reaction at 60 °C. It has been found that reaction does not proceed in presence of reduced graphene oxide sheets and under catalyst free conditions indicating urgent need of the CFRNCs for dibenzylamine product formation. Furthermore, the amount of

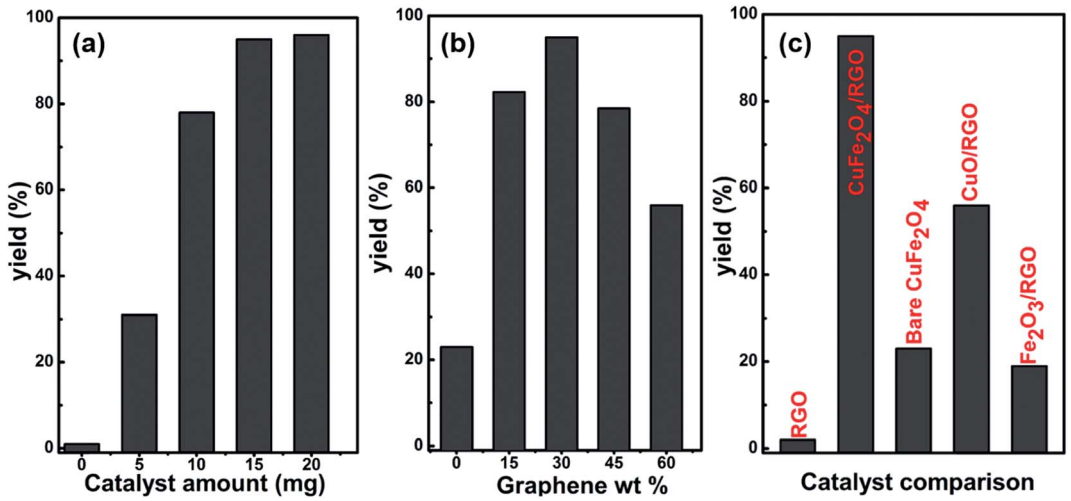

Fig. 4 Comparing the catalytic reactivity with (a) different catalyst amount, (b) effect of intrinsic $CuFe_2O_4$ loading and (c) with different catalysts.

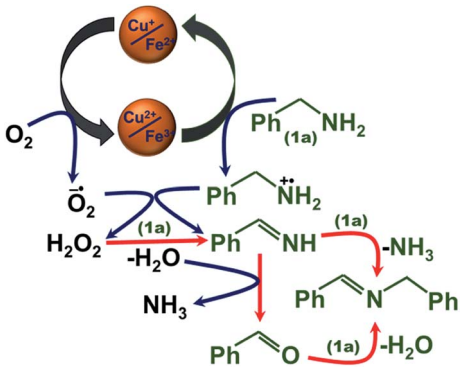

Fig. 5 Proposed catalysis mechanism for aerobic oxidative coupling of amines to imines in presence of CFRNCs.

catalyst was optimized by studying yield obtained *versus* amount of catalyst used (see Fig. 4a).

Since no significant conversion was observed with high catalyst loading of 20 mg while reducing the amount to 15 mg is sufficient to obtain 95% yield of desired imine product with some aldehyde and unidentified impurities just in 8 h. To check the effect of active metal loading, we have synthesized $CuFe_2O_4$/RGO NCs with 15, 30, 45 and 60 wt% graphene by varying the metal precursor amount and characterized by low resolution TEM imaging (see Fig. S5†). As synthesized nanocatalysts were applied in benzylamine oxidation reaction and obtained results are included in Fig. 4b. Since no benzylamine conversion was detected in absence of catalyst, which indicated that $CuFe_2O_4$ NPs were responsible for the oxidation reaction. However, all the $CuFe_2O_4$/RGO samples showed obvious catalytic activity for amine oxidative coupling. When the RGO content in the catalysts increased from 0 to 60%, the benzylamine conversion rate first increased from 23 to 95% and then decreased to 56%. This showed that the introduction of RGO enhanced the catalytic activity of the nanocomposites which is due to uniform dispersity of $CuFe_2O_4$ NPs on RGO sheets and prevented them from agglomerating, thus increasing the number of Cu/Fe active centers. In addition, the π–π stacking and electrostatic interactions between amine and RGO sheets increases the adsorption of reactant on the catalyst and causes increased collision frequency between reactants leading to a high conversion rate. However, decrease in conversion rate with more graphene content (>30 wt%) might be due to lower active content of $CuFe_2O_4$ to provide sufficient active copper/iron centers for oxidative coupling reaction. A significant decrease in imine formation (up to 16%) was found under N_2 environment indicating crucial role of O_2 for happening of catalytic reaction (see Fig. S10† for ^{1}H-NMR data).

3.2. Comparison with separately synthesized catalysts

To understand the catalytic mechanism and high activity of CFRNCs, different nanocatalysts CuO/RGO, Fe_2O_3/RGO, bare $CuFe_2O_4$ and RGO sheets were synthesized under similar reaction condition and catalytic experiments were performed with aerobic oxidative coupling of benzylamine under solvent free conditions (see Fig. 4c). Here CuO/RGO, Fe_2O_3/RGO both catalyzed the reaction and showed imine formation up to 56 and 18% respectively indicating both Cu(II) and Fe(III) as an active centers for coupling reactions. However it can be noticed that $CuFe_2O_4$/RGO NCs with similar loading exhibit higher activity over CuO/RGO and Fe_2O_3/RGO NCs. Based upon these results, the higher activity of CFRNCs may be due to best synergistic effect between $CuFe_2O_4$ NPs/graphene sheets and combined activity of both Cu(II) and Fe(III) metal centers. Similar type of synergistic role of Cu and Fe centers was further supported by earlier reports which explain the better activity of CFRNCs over CuO/RGO and Fe_2O_3/RGO NCs.[15,37] The bare $CuFe_2O_4$ NPs showed only 23% conversion which may be due to absence of graphene sheets causing agglomerated NPs, hence lower surface area (see low resolution TEM in Fig. S6†) while a trace amount of imine product was found in presence of RGO and catalyst free conditions. Based upon above controlled experiments, the high catalytic activity of present CFRNCs nanocatalyst can be ascribed to following factors (1) metal–metal synergy between Cu(II) and Fe(III) metal centers, (2) high surface

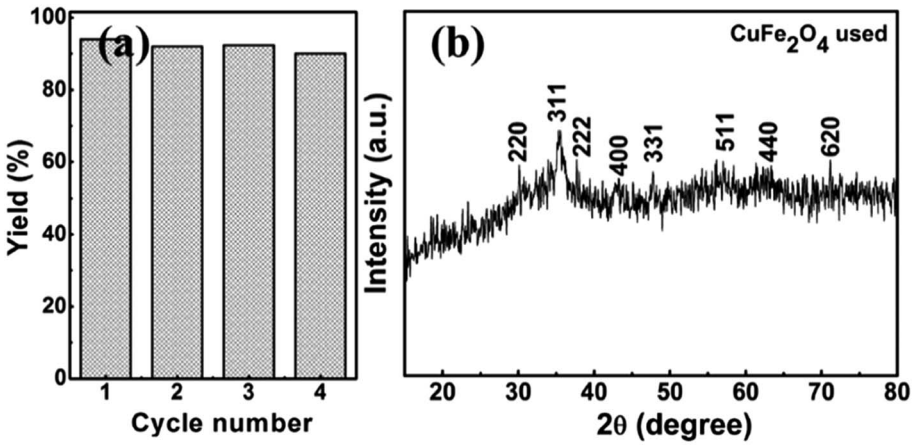

Fig. 6 (a) Recyclability plot showing isolated yield of imine product and (b) powder XRD spectrum of magnetically recovered CFRNCs after 4th catalytic run.

area due to small sized surfactant free $CuFe_2O_4$ NPs and presence of two dimensional graphene sheets and (3) graphene sheets holds organic substrates by π–π interaction with aromatic rings and hence increase the catalytic activity.

3.3. Plausible mechanism

Based upon above controlled experiments and earlier reports, catalytic mechanism of CFRNCs for conversion of amine to imine was proposed which was shown in Fig. 5. In the initial phase both oxygen and amine molecules were activated by both Fe(III) and Cu(II) metal centers and transformed into oxygen and amine radical species which later react to form H_2O_2 and benzylimine intermediates.[3,6] The *in situ* formed H_2O_2 may oxidize another molecule of benzylamine to imine intermediate and get converted into water which later hydrolyze imine to aldehyde.[3] Since the benzylimine intermediate is unstable and its decomposition was further accelerated by Lewis acidic nature of ferrite nanocatalyst. It has been well studied that imine intermediate can decomposed by two pathways, (1) react with another nucleophilic benzylamine molecule to form final product or (2) first hydrolyzed to aldehyde and followed by reaction with another benzylamine molecule to form final desired dibenzylamine product.[8,9] This hypothesis was again proved from NMR results (from reaction course) which showed presence of benzaldehyde.[6] The formation of free radical was also investigated by using 2,2,6,6-tetramethylpiperidine 1-oxyl (TEMPO) as free radical trap which reduces benzylamine conversion up to 2–3% after its addition. This dramatic decrease in conversion confirms the free radical mechanism for this reaction.

3.4. Recyclability and heterogeneity of CFRNCs

To further check the stability and recyclability of CFRNCs, similar catalyst was used up to four consecutive runs under similar reaction condition for aerobic oxidative coupling of benzylamine. After each catalytic cycle, CFRNCs were recovered by magnetic separation, washed, dried and employed for next cycle. The CFRNCs showed very high activity (yield 89%) for amine coupling even after 4th cycle without any accountable loss of activity. Fig. 6a represents the obtained yield after each successive cycle. The recovered catalyst was characterized by powder XRD which showed similar pattern with fresh sample indicating stability of spinel structure (see Fig. 6b). Further, ICP analysis also showed very minute change in percentage loading (0.09%) of copper ferrite NPs. This outstanding stability and recyclability of $CuFe_2O_4$/RGO nanocomposites can be ascribed to very good interaction between ferrite NPs and graphene sheets which prevents agglomeration.

3.5. Substrate scope

With the optimized reaction conditions, we have explored the substrate scope of present nanocatalyst for oxidative coupling reaction and results are shown in Table 1 (see ^{1}H and ^{13}C NMR in Fig. S11–S32†). The present CFRNCs tolerate wide range functional groups and results into desired product with excellent yield for *ortho*, *meta*, *para* substituted electron donating and electron withdrawing groups. The EDG (–CH_3 and –OCH_3) and EWGs (–Cl, –CF_3, –F) on the phenyl ring did not affect the rate of reaction which indicate that there is no clear electronic role of substituents.[3,4] However, for *ortho* and *meta* substituted groups, CFRNCs showed slower reactant conversion which explain stearic effect of substituents. Hence all these outstanding results indicate wide applicability of CFRNCs for such oxidation reactions with excellent activity and high recyclability. Since earlier various heterogeneous materials have been reported for amine to imine conversion, so we have compared our catalyst with some recent metal based heterogeneous catalysts and obtained results are entered in Table S1.† These results indicate that as synthesized CFRNCs are amongst the best heterogeneous catalysts in terms of mild solvent free reaction conditions with high recyclability. Since the TOF values was found higher for Au based catalysts, however inexpensiveness, solvent free catalysis and magnetic recyclability of $CuFe_2O_4$/RGO NCs makes it better for industrial purpose over these catalysts.

Table 1 Oxidative coupling of various amines to imines over CFRNCs[a]

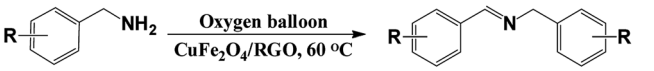

Entry	R	T (h)	Yield[b]
1	H	8	95
2	4-Cl	8	93
3	4-F	8	92
4	2-Me	10	90
5	4-CF_3	8	91
6	4-OMe	8	90
7	4-Me	8	94
8	3-OMe	9	88
9	2-Cl	10	89
10	3,4-Cl	11	89
11	3-CF_3	10	90
12	2-OMe	10	87

[a] Reaction conditions: amine (1 mmol), catalyst (15 mg), O_2 balloon, 60 °C. [b] Isolated yield.

4 Conclusions

$CuFe_2O_4$ NPs were *in situ* synthesized on graphene sheets *via* surfactant free one pot co-precipitation method which exhibited excellent catalytic activity towards self-coupling of amine to imines. The synthesis of NCs was found well controlled by various characterization technique like XRD, TEM, ICP, EDS, FTIR, RAMAN and XPS studies. The CFRNCs catalyzed the aerobic amine coupling under neat conditions just in 8–11 h to get 88–94% isolated yield with excellent selectivity. The CFRNCs were separated magnetically after catalysis reaction and recycled up to four consecutive runs without any accountable loss in activity and stability. In addition, role of Cu, Fe species and graphene sheets in oxidative amine coupling was studied separately by synthesizing CuO/RGO, Fe_2O_3/RGO, bare $CuFe_2O_4$

and RGO sheets. The high catalytic activity of present NCs can be ascribed to high catalytic surface area (due to small sized NPs and graphene sheets), absence of surfactant, excellent synergistic coupling of Cu/Fe species and presence of graphene sheets which holds the organic species by π–π interactions. Hence due to high efficiency and excellent recycling stabilities, CFRNCs may lead to use of present nanocatalyst in many more industrially important catalytic applications.

Acknowledgements

Ritu Dhanda thanks UGC, India for providing senior research fellowship. Authors also thank USIC, DU and SAIF-AIIMS for instrumentation facility and DU R&D for financial support. Authors also acknowledge SAIF-IIT Mumbai for ICP-AES and IIT Delhi for XPS study.

References

1 K. Tanaka and F. Toda, *Chem. Rev.*, 2000, **100**, 1025–1074.
2 A. Loupy, *C. R. Chim.*, 2004, **7**, 103–112.
3 B. Chen, L. Wang, W. Dai, S. Shang, Y. Lv and S. Gao, *ACS Catal.*, 2015, **5**, 2788–2794.
4 S. Biswas, B. Dutta, K. Mullick, C.-H. Kuo, A. S. Poyraz and S. L. Suib, *ACS Catal.*, 2015, **5**, 4394–4403.
5 M. Li, B. Li, H.-F. Xia, D. Ye, J. Wu and Y. Shi, *Green Chem.*, 2014, **16**, 2680–2688.
6 C. Su, R. Tandiana, J. Balapanuru, W. Tang, K. Pareek, C. T. Nai, T. Hayashi and K. P. Loh, *J. Am. Chem. Soc.*, 2015, **137**, 685–690.
7 A. T. Murray, M. J. H. Dowley, F. Pradaux-Caggiano, A. Baldansuren, A. J. Fielding, F. Tuna, C. H. Hendon, A. Walsh, G. C. Lloyd-Jones, M. P. John and D. R. Carbery, *Angew. Chem.*, 2015, **127**, 9125–9128.
8 X.-J. Yang, B. Chen, X.-B. Li, L.-Q. Zheng, L.-Z. Wu and C.-H. Tung, *Chem. Commun.*, 2014, **50**, 6664–6667.
9 Y. Zhang, L. Pei, Z. Zheng, Y. Yuan, T. Xie, J. Yang, S. Chen, J. Wang, E. R. Waclawik and H. Zhu, *J. Mater. Chem. A*, 2015, **3**, 18045–18052.
10 H. Liu, G.-K. Chuah and S. Jaenicke, *J. Catal.*, 2015, **329**, 262–268.
11 M. Gohain, V. Kumar, J. H. van Tonder, H. C. Swart, O. M. Ntwaeaborwa and B. C. B. Bezuidenhoudt, *RSC Adv.*, 2015, **5**, 18972–18976.
12 S. Paul, G. Pal and A. R. Das, *RSC Adv.*, 2013, **3**, 8637–8644.
13 A. L. García-Cabeza, R. Marín-Barrios, F. J. Moreno-Dorado, M. J. Ortega, H. Vidal, J. M. Gatica, G. M. Massanet and F. M. Guerra, *J. Org. Chem.*, 2015, **80**, 6814–6821.
14 S. Ahammed, D. Kundu and B. C. Ranu, *J. Org. Chem.*, 2014, **79**, 7391–7398.
15 C.-C. Kuan, S.-Y. Chang and S. L. M. Schroeder, *Ind. Eng. Chem. Res.*, 2015, **54**, 8122–8129.
16 A. S. Kumar, M. A. Reddy, M. Knorn, O. Reiser and B. Sreedhar, *Eur. J. Org. Chem.*, 2013, **2013**, 4674–4680.
17 T. Zhang, H. Zhu and J.-P. Croué, *Environ. Sci. Technol.*, 2013, **47**, 2784–2791.
18 Y. Feng, D. Wu, Y. Deng, T. Zhang and K. Shih, *Environ. Sci. Technol.*, 2016, **50**, 3119–3127.
19 R. Zhang, C. Miao, Z. Shen, S. Wang, C. Xia and W. Sun, *ChemCatChem*, 2012, **4**, 824–830.
20 A. T. Nguyen, L. T. M. Nguyen, C. K. Nguyen, T. Truong and N. T. S. Phan, *ChemCatChem*, 2014, **6**, 815–823.
21 Y. Zhao, G. He, W. Dai and H. Chen, *Ind. Eng. Chem. Res.*, 2014, **53**, 12566–12574.
22 Y. Fu, Q. Chen, M. He, Y. Wan, X. Sun, H. Xia and X. Wang, *Ind. Eng. Chem. Res.*, 2012, **51**, 11700–11709.
23 W. Zhang, B. Quan, C. Lee, S.-K. Park, X. Li, E. Choi, G. Diao and Y. Piao, *ACS Appl. Mater. Interfaces*, 2015, **7**, 2404–2414.
24 H. Zhang, S. Gao, N. Shang, C. Wang and Z. Wang, *RSC Adv.*, 2014, **4**, 31328–31332.
25 C. N. R. Rao, A. K. Sood, K. S. Subrahmanyam and A. Govindaraj, *Angew. Chem., Int. Ed.*, 2009, **48**, 7752–7777.
26 A. K. Geim and K. S. Novoselov, *Nat. Mater.*, 2007, **6**, 183–191.
27 A. Peigney, C. Laurent, E. Flahaut, R. R. Bacsa and A. Rousset, *Carbon*, 2001, **39**, 507–514.
28 J. C. Reed, H. Zhu, A. Y. Zhu, C. Li and E. Cubukcu, *Nano Lett.*, 2012, **12**, 4090–4094.
29 L. Britnell, R. V. Gorbachev, R. Jalil, B. D. Belle, F. Schedin, A. Mishchenko, T. Georgiou, M. I. Katsnelson, L. Eaves, S. V. Morozov, N. M. R. Peres, J. Leist, A. K. Geim, K. S. Novoselov and L. A. Ponomarenko, *Science*, 2012, **335**, 947–950.
30 X. Zhu, Y. Zhu, S. Murali, M. D. Stoller and R. S. Ruoff, *ACS Nano*, 2011, **5**, 3333–3338.
31 H. Zhang, X. Lv, Y. Li, Y. Wang and J. Li, *ACS Nano*, 2010, **4**, 380–386.
32 R. Dhanda and M. Kidwai, *J. Mater. Chem. A*, 2015, **3**, 19563–19574.
33 D. C. Marcano, D. V. Kosynkin, J. M. Berlin, A. Sinitskii, Z. Sun, A. Slesarev, L. B. Alemany, W. Lu and J. M. Tour, *ACS Nano*, 2010, **4**, 4806–4814.
34 F. Meng, J. Li, S. K. Cushing, J. Bright, M. Zhi, J. D. Rowley, Z. Hong, A. Manivannan, A. D. Bristow and N. Wu, *ACS Catal.*, 2013, **3**, 746–751.
35 Y. Xu, H. Bai, G. Lu, C. Li and G. Shi, *J. Am. Chem. Soc.*, 2008, **130**, 5856–5857.
36 F. Tuinstra and J. L. Koenig, *J. Chem. Phys.*, 1970, **53**, 1126.
37 G. Rong, J. Mao, H. Yan, Y. Zheng and G. Zhang, *J. Org. Chem.*, 2015, **80**, 4697–4703.